International Communications in Heat and Mass Transfer 133 (2022) 105923

Contents lists available at ScienceDirect

International Communications in Heat and Mass Transfer

journal homepage: www.elsevier.com/locate/ichmt

An entropy generation analysis of horizontal convection under the centrifugal buoyancy approximation

Peyman Mayeli *, Gregory J. Sheard

Department of Mechanical and Aerospace Engineering, Monash University, VIC 3800, Australia

ARTICLE INFO

Keywords:
Horizontal convection
Centrifugal buoyancy approximation
Gay-Lussac parameter
Entropy generation analysis

ABSTRACT

An entropy generation analysis is conducted for horizontal convection under the centrifugal buoyancy and the Boussinesq approximations in a relatively shallow enclosure at a fixed Prandtl number of unity to characterise irreversible losses across the conduction and convection-dominated regimes using the Bejan number (Be). A variable irreversibility distribution factor is expressed for the entropy generation analysis as a ratio of the Brinkman number (Br) and the Gay-Lussac (Ga) parameter for the first time. Governing equations are solved numerically using a high-order nodal spectral-element method. Calculations are performed at a fixed $Br = 2 \times 10^{-5}$ over the physical range of the Gay-Lussac parameter $0 \leq Ga \leq 2$ up to $Ra = 5 \times 10^8$. As expected, increasing the Rayleigh number shifts the flow toward a convection-dominated regime; however it is found that increasing the Gay-Lussac parameter draws the heat transfer mechanism back to a conduction-dominated state. In other words, advection related buoyancy effects act to keep the buoyancy-driven flow in conduction-dominated regime. The entropy generation analysis indicates that at $Ga \gtrsim 0.5$ conduction and convection are in balance at $Ra \approx 6 \times 10^5$, while under the conventional Boussinesq approximation ($Ga = 0$), heat transfer is convection-dominated. The transition of the average Bejan number from conduction to convection-dominated regime follows closely to a reciprocal scaling against Rayleigh number $Be_{ave} \sim Ra^{-1}$ when $Ga = 0$ but the same process scales with $Be_{ave} \sim Ra^{-0.5}$ relation at $Ga = 2$.

1. Introduction

Horizontal convection (HC) refers to natural convection in which fluid motion is invoked by non-uniform buoyancy long a horizontal buoyancy. In HC, the fluid is overturning at any Rayleigh number due to horizontal non-uniformity in buoyancy [1]. This type of convection is of interest due to its contribution in geological applications such as oceanic [2] and atmospheric [3] flow patterns as well as industrial application such as glass melting [4].

Some studies have been conducted for HC. One of the pioneering studies in HC is Rossby's $Nu \sim Ra^{1/5}$ scaling [5] in the convection dominated regime. The same scaling for the average Nusselt number against the Rayleigh number is reported up to $Ra = O(10^9)$ by Siggers et al. [6] and Sheard and King [7]. Shishkina et al. [8] adapted the scaling theory developed by Grossmann and Lohse [9] for Rayleigh–Bénard convection to a HC system where global averaged kinetic and thermal dissipation rates are decomposed into boundary layer and bulk contributions. Their theory verifies Rossby's scaling [5], characterised by the thermal boundary layer being thicker than the kinetic layer, and both thermal and kinetic dissipation being dominant in the boundary layers. A fairly comprehensive review about different aspect of HC has been provided by Hughes and Griffiths [10].

In the literature, HC systems have been studied under the classical Boussinesq approximation where density differences are considered only in the gravity term. This assumption impedes application to problems featuring large temperature differences, rapid rotation, etc. [11]. One approach that extends this treatment is the Gay-Lussac (Ga) approach in which the density variations are reintroduced wherever density appears in the governing equations [12–14]. The Gay-Lussac parameter $Ga = \beta \Delta\theta$, as a product of temperature difference and isobaric expansion coefficient emerges from this treatment. The centrifugal approximation [15–16] is a subcategory of the Gay-Lussac approach in which the density variations are extended to the advection terms of the momentum equation as well as the gravity term. This approach is suitable for flows having either localised or global rapid rotation. The interested reader is directed to a recent review of buoyancy models within and outside the Boussinesq approximation [17]. More recently, Mayeli et al. [18] studied HC under the centrifugal buoyancy approximation, finding that in the range of $4.23 \times 10^8 \leq Ra \leq 6.5 \times 10^8$

* Corresponding author.
E-mail addresses: Peyman.Mayeli@monash.edu (P. Mayeli), Greg.Sheard@monash.edu (G.J. Sheard).

https://doi.org/10.1016/j.icheatmasstransfer.2022.105923

Available online 16 February 2022

Nomenclature

Be_{ave}	average Bejan number
Be_{loc}	local Bejan number
Br	Brinkman number
e_g	unit vector in gravity direction
g	gravitational acceleration (m/s^2)
Ga	Gay-Lussac parameter ($\beta\Delta\theta$)
k	thermal conductivity ($W/m.K$)
L_{ref}	reference length (m)
n	normal vector of the surface
p	Pressure (Pa)
p^*	modified pressure
P	dimensionless pressure
Pr	Prandtl number
q	Heat (W)
$q_{cond.}$	conducted heat
$q_{visc.\ dissip.}$	dissipated heat due to viscosity
Ra	Rayleigh number
S_Θ	entropy generation due to heat transfer
S_ψ	entropy generation due to fluid friction
T	Temperature (K)
x	Cartesian coordinate (m)
X	dimensionless Cartesian coordinate
u	velocity vector (m/s)
U	dimensionless velocity vector
α	thermal diffusivity (m^2/s)
β	isobaric expansion coefficient ($1/K$)
θ	physical temperature (K)
$\Delta\theta$	reference temperature difference (K)
Θ	dimensionless temperature
ε	relative temperature difference
μ	dynamic viscosity ($Pa.s$)
ρ	density (kg/m^3)
ρ_0	reference density (kg/m^3)
τ_w	wall shear stress (Pa)
χ	irreversibility distribution ratio

Subscript

ave	average
c	cold
h	hot
loc	local
tot	total
0	a reference value

there exists a physical Ga that beyond which the buoyancy-driven flow becomes unstable.

In this study, the centrifugal approximation provides the basis for an entropy generation analysis in HC. A literature survey indicates that entropy generation analysis has not been applied to any HC problem before, but there are a vast number of studies in which different thermo-flow fields have been analyzed in terms of entropy generation. Interested readers are referred to the recent review paper [19] for a detailed discussion of entropy generation of nanofluid and hybrid nanofluid flow in thermal systems. In ref. 19 it is concluded that for microchannel systems, entropy generation decreases with decreasing nanoparticle size or increasing concentration. Also for open cavities, the entropy generation decreases by increasing both the Hartmann number and volume fraction at horizontal magnetic field, thus application direction of magnetic field is important to minimize the entropy generation.

Tayebi et al. [20–23] performed entropy generation analysis of natural convection in different setups such as square cavity with a conducting hollow cylinder [20] concluding that inserting a hollow conducting cylinder plays an important role in controlling flow characteristic and irreversibilities within the cavity. An entropy generation analysis in an annular enclosure fitted with fins under magnetic field effects [21], led to concluding irreversibility related to thermo-effects is predominant at low Rayleigh numbers, while at high Rayleigh numbers, the irreversibility due to heat transfer is no longer the main contributor of overall entropy production. Their results indicate that the in the presence of magnetic, increase the share of heat transfer irreversibility in total entropy generation. Tayebi and Oztop [22] investigated free convection in horizontal confocal elliptic cylinders filled with Al_2O_3-Cu/water hybrid nanofluid. An important contribution of their work was finding the average Bejan number is not affected by the addition of hybrid nanoparticles. Tayebi et al. [23] studied free convection in annular elliptical cavity filled with Al_2O_3-Cu/water hybrid nanofluid with an internal heat generator/absorber. They found that in the case of heat absorption, reduction of the average Bejan number by increasing Rayleigh number is more gradually and adding nanoparticles doesn't apply much effect on the average Bejan number. Dutta et al. [24] analysed free convection heat transfer in a rhombic enclosure using Cu-water working nanofluid under the magnetic field effects. Findings of their study indicates that the rate of total entropy generation has a revers relation with Hartman number and leaning angles of the geometry.

Many entropy generation analysis is also preformed in the sister class of free convection i.e. mixed convection under the Boussinesq approximation. Alsabery et al. [25] studied entropy generation analysis in an enclosure with wavy horizontal walls having different number of undulations and a rotating cylinder at the center of chamber. They found that for different number of undulations, the Bejan number is the highest for the case involving a nearly stationary inner cylinder. Hussein [26] performed an entropy generation analysis due to the transient mixed convection in a 3D right-angle triangular cavity concluding that the flow field inside the cavity is influenced significantly with the direction of the moving wall. It is also found that the Bejan number decreases as the Richardson number increases. Al-Rashed et al. [27] conducted an entropy generation analysis in a 3D heated up cubical open cavity containing a central isothermal block using vorticity-velocity approach. Their simulations were performed over Richardson number 0.01–100 and percentage of Al_2O_3 nanoparticles 1–5%, concluding that the thermal entropy generation increases by increasing the concentration of nanoparticles for all Richardson numbers, but the variation of viscous entropy generation with concentrations depends on Richardson number value. Ghachem and co-workers [28] performed a numerical simulation of 3D double-diffusive free convection and studied irreversibility effects in a solar distiller. They found that all kinds of entropy generations present a minimum value when buoyancy forces due to density and concentration differences are equal. They reported total entropy rises considerably by increasing buoyancy forces ratio. Hussein et al. [29] studied unsteady laminar 3D natural convection and entropy generation in an inclined cubical trapezoidal air-filled cavity for $10^3 \leq Ra \leq 10^5$ and different inclination angle from 0^o to 180^o. They found that the inclination angle has almost no effect on the total entropy generation in conduction-dominated regime. Al-Rashed, et al. [30] investigated entropy generation for air in a 3D cubical cavity with partially active vertical walls and four different arrangements of heating and cooling section up to $Ra = 10^6$. They found that the arrangements of heating and cooling regions have a significant effect on the entropy generation. They also reported cases corresponding to minimum and maximum Bejan number among four considered cases for their study.

Entropy generation is also investigated for buoyancy-driven flows in porous medium. For instance, Dutta et al. [31] surveyed variation of

entropy generation in a porous quadrantal enclosure with non-uniform thermal condition. Their findings indicates entropy generation due to heat transfer is the significant contributor of irreversibility at low values of Darcy number, while for larger values of Darcy number and Rayleigh number viscous dissipation becomes dominant part of total entropy generation. A similar study is also performed on a porous rhombic enclosure [32]. Bhardwaj et al. [33] studied free convection in a porous triangular enclosure with a wavy vertical wall using vorticity stream-function approach. Their numerical results indicates that by increasing the Darcy number, conduction dominates heat transfer mechanism. They also reported that entropy generation in the presence of undulations is significantly higher compared to the situation with a flat wall, while irreversibilities due to heat transfer is almost equal for both scenarios.

In all aforementioned works [20–33], the Boussinesq approximation for buoyancy-driven flows serves as a fundamental assumption for governing equation. In this study, findings of the stability analysis of HC under the centrifugal buoyancy approximation [18] are extended by determining different conduction and convection-dominated regimes and the effect of Ga on the local and global entropy generation. In the next section, the governing equations under the centrifugal approximation are introduced. Section 3 deals with the numerical set up and treatment of the irreversibility distribution ratio. Results are presented in Section 4, and in Section 5, a short conclusion is drawn.

2. Governing equations under the centrifugal buoyancy approximation

The centrifugal approximation follows fundamentals of the classic Boussinesq approximation but it extends the density variations to the advection term in addition to gravity term of the momentum equation, offering an improved description of rotation in a buoyancy-driven flow [15–16]. The dimensional form of the governing equations under the centrifugal approximation may be expressed as,

$$\nabla\bullet \mathrm{u} = 0, \tag{1}$$

$$\partial u/\partial t^{*} + (\rho/\rho_0)(u\bullet\nabla)\mathrm{u} = -(1/\rho_0)\nabla \mathrm{p} + \nu\nabla^2\mathrm{u} + (\rho/\rho_0)\mathrm{ge_g}, \tag{2}$$

$$\partial T/\partial t^{*} + (u\bullet\nabla)\mathrm{T} = \alpha\nabla^2\mathrm{T}, \tag{3}$$

where using the following non-dimensionlised quantities,

$$t = \frac{t^{*}\alpha}{L^2}, X = \frac{x}{L_{ref}}, U = \frac{uL_{ref}}{\alpha}, P = \frac{p^{*}{L_{ref}}^2}{\rho\alpha^2}, \Theta = \frac{\theta}{\Delta\theta} = \frac{T - T_0}{T_h - T_c}, Ga = \beta\Delta\theta, \tag{4}$$

accompanied by a linear density state relation ($\rho/\rho_0 = 1 - \beta\theta$), yields the dimensionless form of the governing equations,

$$\nabla\bullet \mathrm{U} = 0, \tag{5}$$

$$\partial U/\partial t + (U\bullet\nabla)\mathrm{U} = -\nabla \mathrm{P} + \mathrm{Pr}\nabla^2\mathrm{U} - \mathrm{RaPr}\Theta\mathrm{e_g} + \mathrm{Ga}\Theta(\mathrm{U}\bullet\nabla)\mathrm{U}, \tag{6}$$

$$\partial\Theta/\partial t + (U\bullet\nabla)\Theta = \nabla^2\Theta, \tag{7}$$

that are solved by considering the following boundary conditions,

$$U = 0 \text{ on } Y = 0, 0.16 \text{ and } -0.5 \le X \le 0.5, \tag{8}$$

$$U = 0 \text{ on } X = -0.5, 0.5 \text{ and } 0 \le Y \le 0.16, \tag{9}$$

$$\Theta = X - 0.5 \text{ on } Y = 0 \text{ and } -0.5 \le X \le 0.5, \tag{10}$$

$$\partial\Theta/\partial n = 0 \text{ on } Y = 0.16 \text{ and } -0.5 \le X \le 0.5, \tag{11}$$

$$\partial\Theta/\partial n = 0 \text{ on } X = -0.5, 0.5 \text{ and } 0 \le Y \le 0.16. \tag{12}$$

Eqs. (5)–(7) introduce the Gay-Lussac parameter $Ga = \beta\Delta\theta$ (incidentally being twice the relative temperature difference, $Ga = 2\varepsilon$), a Rayleigh number characterising the ratio of buoyancy to thermal and viscous dissipation, $Ra = g\beta\Delta\theta{L_{\mathrm{ref}}}^3/\nu\alpha$, and the Prandtl number characterising the ratio of viscous to thermal dissipation, $Pr = \nu/\alpha$. In Eq. (4) $T_0 = 0.5(T_h - T_c)$ and the reference length is equal to the horizontal length of HC system. In addition, p^{*} is a modified pressured that absorbs the hydrostatic pressure effects i.e. $p^{*} = p + \rho_0\phi$, where ϕ is the gravitational potential.

The centrifugal approximation is consistent with the conventional Boussinesq approximation, except for the additional inertial buoyancy term on the right-hand side of the momentum equation arising as a consequence of extending the density variations beyond the gravity term. Ga also appears in the dimensionless form of the density state relation,

$$\rho/\rho_0 = 1 - \beta\theta = 1 - \beta\Delta\theta\Theta = 1 - Ga\Theta. \tag{13}$$

and its range is limited to $0 \le Ga \le 2$ to avoid negative density ratios.

3. Problem description and numerical setup

The centrifugal approximation is applied to HC problem in a rectangular enclosure with a fixed aspect ratio $A = H/L = 0.16$. An invariant unit Prandtl number $Pr = 1$ is considered, applicable to fluids including air and steam. A schematic of the enclosure and applied boundary conditions is presented in Fig. 1a. A linear temperature variation is applied along the bottom boundary while other surfaces are thermally insulated. This configuration cools and heats the fluid over the left and right regions of the bottom boundary, respectively. This buoyancy imbalance leads to the formation of a counter clock-wise overturning circulation. For this problem, it is supposed that the buoyancy-driven flow is 2D and laminar and the working fluid circulating inside the enclosure is Newtonian. In the considered range of the dominant parameters ($0 \le Ga \le 2$, $Pr = 1$ and $10^2 \le Ra \le 5 \times 10^8$), all flow simulations lead to a steady-state solution.

Eqs. (1)–(3) are solved using a high-order nodal spectral-element method with time integration via a third-order backward differentiation scheme. In spectral-element method, physical domain is discretised by overlapping elements and a continuous Galerkin method is applied that leads to a weak form of the governing equations. For high accuracy purposes, an orthonormal basis function such as Legendre polynomials is used in the Galerkin formulation and resultant equations are integrated over space using Gaussian quadrature formula (Gauss-Lobatto-Legendre). Indeed, spectral-element method combines the accuracy of spectral methods with the geometrical flexibility of finite elements that yields an efficient computational method in which the error decreases exponentially as the order of approximating polynomial increases.

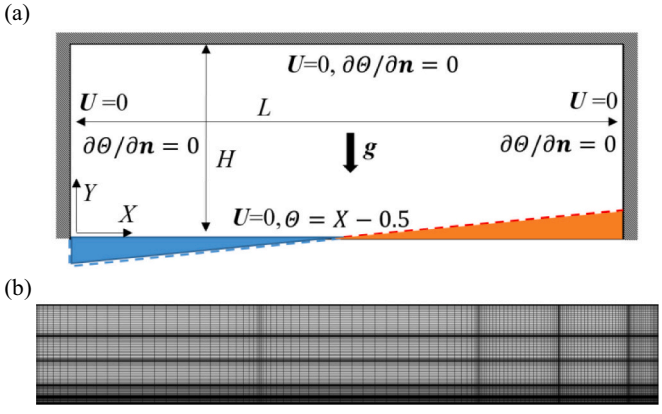

Fig. 1. (a) A schematic depiction of the horizontal convection problem showing the imposed boundary conditions, (b) The mesh showing interior quadrature points within the 5 × 4 spectral elements.

Meshing the physical geometry is performed so that resolution is concentrated toward the bottom boundary and towards the heating section where buoyancy is expected to produce plume structures. This is performed with a small number of elements having a high polynomial order 30. The mesh independency is checked in terms of an L_2 norm (defined as the integral of the velocity magnitude over the physical domain) and it is found that over the considered parameter range is less than 2×10^{-7}% [18].

Entropy generation analysis is an effective technique that can distinguish the evolution of heat transfer mechanism from conduction to convection both locally and globally. This is performed by measuring the entropy generation due to viscous and thermal dissipation in the context of the Bejan number, where the viscous contribution is associated with convective motions in the fluids [34]. Indeed, heat transfer processes inevitably encounter irreversible loss of useful work via dissipative processes that generate entropy. Understanding the sources of entropy generation in heat transfer may therefore provide insights permitting the improvement of efficiency in systems featuring such heat transfer processes. Following Ref. 34, for incompressible fluids in the absence of internal heating, local volumetric entropy generation (here normalised by $T_0^2L^2/k\Delta\theta^2$) may be expressed as,

$$S^{'''} = S_\Theta + \chi S_\psi \tag{14}$$

where the respective contributions due to thermal conduction and viscous friction are [34]

$$S_\Theta = \left[\left(\frac{\partial \Theta}{\partial X}\right)^2 + \left(\frac{\partial \Theta}{\partial Y}\right)^2\right], \tag{15}$$

$$\chi S_\psi = \chi\left[2\left\{\left(\frac{\partial U}{\partial X}\right)^2 + \left(\frac{\partial V}{\partial Y}\right)^2\right\} + \left(\frac{\partial U}{\partial Y} + \frac{\partial V}{\partial X}\right)^2\right], \tag{16}$$

and the irreversibility distribution ratio is $\chi = \mu T_0\alpha^2/kL^2\Delta\theta^2$. The irreversibility factor may be also expressed as,

$$\chi = \mu {u_0}^2 \times \frac{1}{(k\Delta\theta)} \times \left(\frac{T_0}{\Delta\theta}\right) = u_0 \frac{(\mu u_0)}{(k\Delta\theta)} \times \left(\frac{T_0}{\Delta\theta}\right) = u_0 \frac{\left(\frac{\mu u_0}{L}\right)}{\left(\frac{k\Delta\theta}{L}\right)} \times \left(\frac{T_0}{\Delta\theta}\right)$$

$$= \frac{(u_0\tau_w)}{(q_{cond})} \times \left(\frac{T_0}{\Delta\theta}\right),$$

or in other words,

$$\chi = \frac{q_{visc.dissip.}}{q_{cond.}} \times \frac{1}{Ga} = \frac{Br}{Ga}. \tag{17}$$

Eq. (17) demonstrates that the irreversibility distribution ratio may be expressed in terms of the Brinkman number characterising the ratio of the viscous heat dissipation to heat conduction within the system. Typically, a small value is employed for the irreversibility distribution ratio. Considering $\chi = 10^{-4}$ (consistent with refs. [26, 28, 30]) under the Boussinesq approximation with relative temperature difference $\varepsilon = 0.01$ ($Ga = 0.02$), gives $Br = 2 \times 10^{-5}$. In this study, we alter the irreversibility distribution corresponding to different Ga at a fixed $Br = 2 \times 10^{-5}$.

The ratio of entropy generation due to thermal conduction to total entropy generation yields the local Bejan number,

$$Be_{loc} = \frac{S_\Theta}{S_\Theta + \chi S_\psi}, \tag{18}$$

from which the mean over the enclosure is obtained from

$$Be_{\mathrm{ave}} = \frac{L}{H}\int_\Omega Be_{\mathrm{loc}}\, d\Omega. \tag{19}$$

In entropy generation analysis, $Be > 0.5$ corresponds to scenarios where entropy generation is dominated by dissipation via thermal conduction, whereas $Be < 0.5$ corresponds to scenarios where entropy generation is dominated by viscous friction, correlating with convective heat transport.

4. Entropy generation analysis

For the entropy generation analysis in this study, calculations are performed over $10^2 \le Ra \le 5 \times 10^8$ at $Ga = 0$, 0.5, 1, 1.5 and 2. Sections 4.1 and 4.2, deal with the global and local irreversibilities, respectively, as well as the average and local Bejan number,

4.1. The effect of the Gay-Lussac parameter on the total irreversibilities and the average Bejan number

The effects of the different Ga on the $S_{\Theta tot}$, $\chi S_{\psi tot}$ and Be_{ave} are investigated in Fig. 2. Here, $S_{\Theta tot}$ and $\chi S_{\psi tot}$ refer to the integral of local S_Θ and χS_ψ over the physical domain, respectively. For entropy generation due to thermal diffusion, two regions are detected in Fig. 2a; in which up to $Ra \approx 10^6$, $S_{\Theta tot}$ remains constant, while in the second region $10^6 \lesssim Ra \le 5 \times 10^8$, it grows almost linearly. It should be noted that, the increase in $S_{\Theta tot}$ is modest being only approximately 30 times larger at $Ra = 5 \times 10^8$ than at $Ra = 10^2$ for different Ga. As seen, entropy generation due to thermal diffusion grows faster for the smaller Ga in the second region.

For entropy generation due to fluid friction (Fig. 2b), two regions are detectable. $\chi S_{\psi tot}$ increases quadratically with Ra up to $Ra \approx 10^6$ for all Ga. Subsequently, there is a linear power law correlation in the range of $10^7 \le Ra \le 5 \times 10^8$ at $Ga = 0$. This slope decreases slightly as Ga is increased, to an exponent of approximately 0.9.

Variation of the average Bejan number against Rayleigh number is presented in Fig. 2c. A feature of this figure is the intersection of the average Bejan number at different Ga with $Be_{ave} = 0.5$ that indicates conduction and convection are in balance with respect to heat transfer. At $Ga = 0$, this occurs at $Ra \approx 4 \times 10^4$, but by increasing Ga, the corresponding Rayleigh number shifts to a higher value. In other words, higher Ga tends to delay the migration from conduction to convection-dominated regime. For instance, at $Ga = 2$ intersection with $Be_{ave} = 0.5$ occurs at $Ra \approx 7 \times 10^5$. Beyond the $Be_{ave} = 0.5$ crossing, at $Ga = 0$ the average Bejan number follows closely to a reciprocal ($Be_{ave} \sim Ra^{-1}$) scaling. However, the same process occurs with a softer $Be_{ave} \sim Ra^{-0.5}$ relation at $Ga = 2$. In general, as Rayleigh number is increased into the convection-dominated regime, the average Bejan number decreases. This behaviour comes from the Bejan number definition as it is defined as the ratio of entropy generation due to thermal conduction to total entropy generation as the summation of the thermal conduction and viscous dissipation irreversibilities. Higher Rayleigh numbers are associated with stronger buoyancy forces that generates larger velocity gradients and consequently larger irreversibilities due to fluid friction that yields smaller Bejan number.

Results demonstrate that the effect of the Ga on the average Bejan number is negligible in the conduction dominated regime ($Ra \lesssim 10^4$), but it becomes significant in the fully convection-dominated regime, so much so that the difference of Be_{ave} at the largest calculated Rayleigh number at $Ra = 5 \times 10^8$ is around 95% between $Ga = 0$ and 2. Finally, in the fully convection-dominated regime ($Ra \ge 10^7$), the average Bejan number at $Ga = 0$ correlates close to $Be_{ave} \sim Ra^{-1/3}$, however this ratio decreases with increasing Ga such that a $Be_{ave} \sim Ra^{-0.3}$ relation is obtained by $Ga = 2$. A scaling of $Ra^{-1/3}$ is not unfamiliar in the context of horizontal convection. In HC, Nusselt number scales as the reciprocal HC boundary layer thickness. Siggers et al. [6] performed a variational analysis that revealed a lower bound on the scaling of the horizontal convection boundary layer thickness with Rayleigh number as $Ra^{-1/3}$. Separately, Shishkina et al. [8] developed a theory for the scaling of heat transport in horizontal convection based on an analysis of respective rates of thermal and kinetic dissipation in both the boundary layer and the interior. They proposed a Nusselt number regime scaling as $Nu \sim Ra^{1/}$

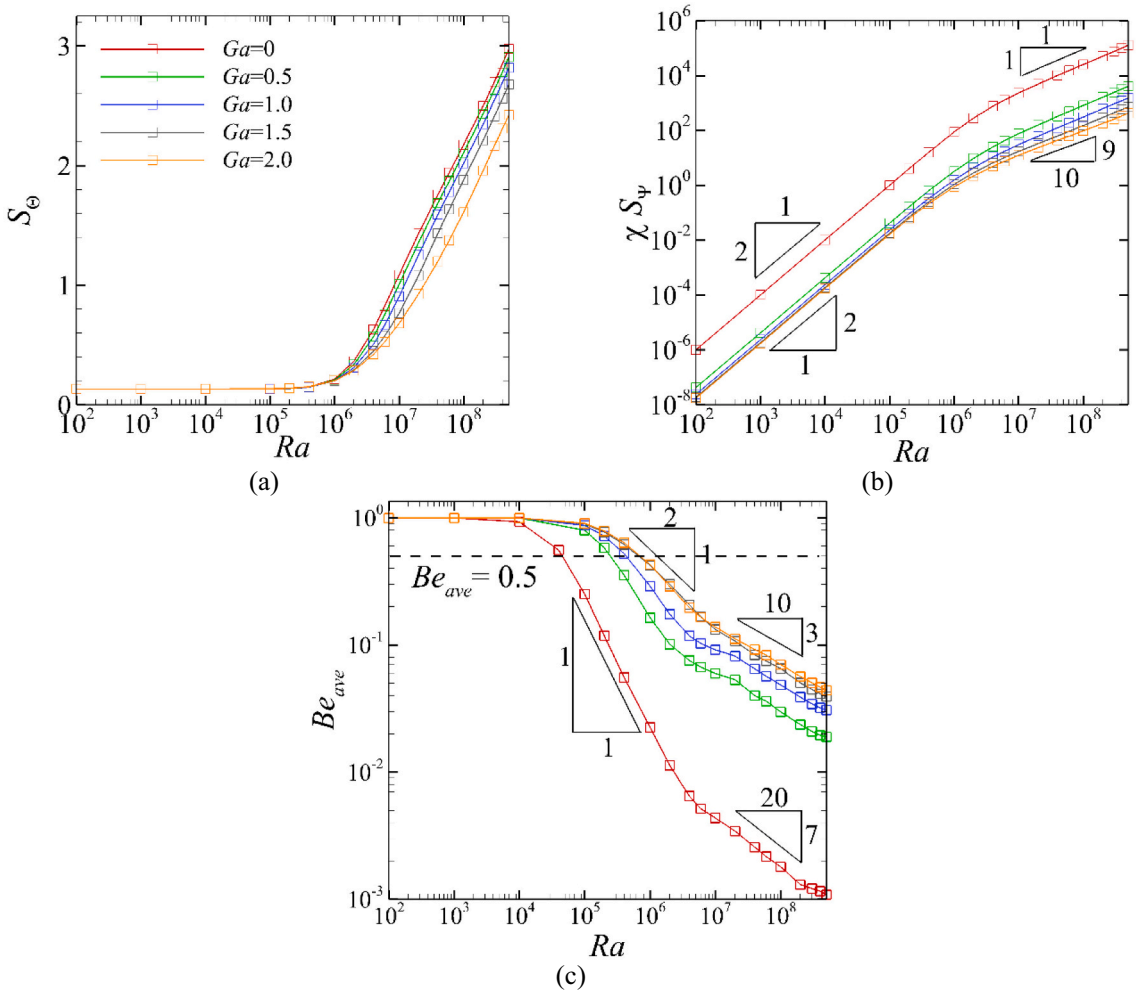

Fig. 2. Variation of different entropy related parameters against the Rayleigh number at different *Ga* including (a) Entropy generation due to heat transfer (b) Entropy generation due to fluid friction (c) Average Bejan number. Indicators of power-law exponent gradients are included for reference.

[3] (i.e. the reciprocal of the aforementioned $Ra^{-1/3}$ scaling) arising from the scenario whereby kinetic and thermal dissipation rates were both dominant within the interior rather than the boundary layer.

4.2. The effect of the Gay-Lussac parameter on the local irreversibilities and local Bejan number

To probe further, four Rayleigh numbers are selected and the rates of the local irreversibilities and the local Bejan number are scrutinized in detail at different *Ga* in the analysis to follow. These four Rayleigh numbers cover different regimes so that a Rayleigh number is selected from conduction dominated regime, one Rayleigh number is near $Be_{ave} = 0.5$ and two Rayleigh numbers are selected from the convection-dominated regime.

Fields of the local entropy generation due to fluid friction (S_ψ) are portrayed in Fig. 3. Results indicates that, in the conduction-dominated regime (Fig. 3a), S_ψ is small overall, with largest values being found adjacent to the top and bottom boundaries. A weaker zone extends centrally through the interior. This field is largely absent at right sidewall of the enclosure. In this regime, the apparent effect of *Ga* is to increase S_ψ over the cooling section. Fig. 3b represents S_ψ at $Ra = 6 \times 10^5$ (in the vicinity of $Be_{ave} = 0.5$ for most of *Ga* values except $Ga = 0$ in Fig. 2c) where the irreversibilities due to heat transfer and fluid friction are in balance. Here, while the patterns are similar S_ψ is three orders of magnitude larger than $Ra = 10^4$. In this regime, though its distribution is consistent, with the exception being slightly stronger values in the interior zone, increasing *Ga* draws larger S_ψ toward the cooling section with more strength meaning convection is becoming stronger at this region.

At the convection-dominated regime $Ra = 4 \times 10^7$ and 4×10^8 (Fig. 3c and d), S_ψ is two to three orders of magnitude larger than $Ra = 6 \times 10^5$. In this regime, convection effects S_ψ adopts a different distribution. It is relatively much stronger along the bottom boundary than the top likely due to the friction of the HC boundary layer adjacent to the bottom surface, and the interior zone has contracted and shifted downward and to the hot end of the enclosure. This reflects skewing of the overturning flow towards the lower-right of the enclosure [7] as the dark color shows stronger convection-dominated region. In other words, as the fluid moves relatively parallel to the bottom boundary, it receives stronger buoyancy forces by approaching to the bottom right corner as a linear temperature distribution is imposed along the bottom boundary. The location where the working fluid receives maximum energy coincidences with the region that it has to rotate due to geometry confinement. This generates large velocity gradients compared to other regions and consequently larger irreversibilities due to fluid friction.

Excitingly, significant *Ga*-dependence is reversed in the convection-dominated regime (Fig. 3a and b) compared to conduction-dominated regime (Fig. 3a and b). Strong entropy generation in the ascending plume adjacent to the right wall is seen at $Ga = 0$, though this becomes progressively weaker as *Ga* increases; being almost absent beyond $Ga \approx 1.5$. The strength of S_ψ in the interior zone also weakens as *Ga* is increased. These results suggest that centrifugal buoyancy effects are

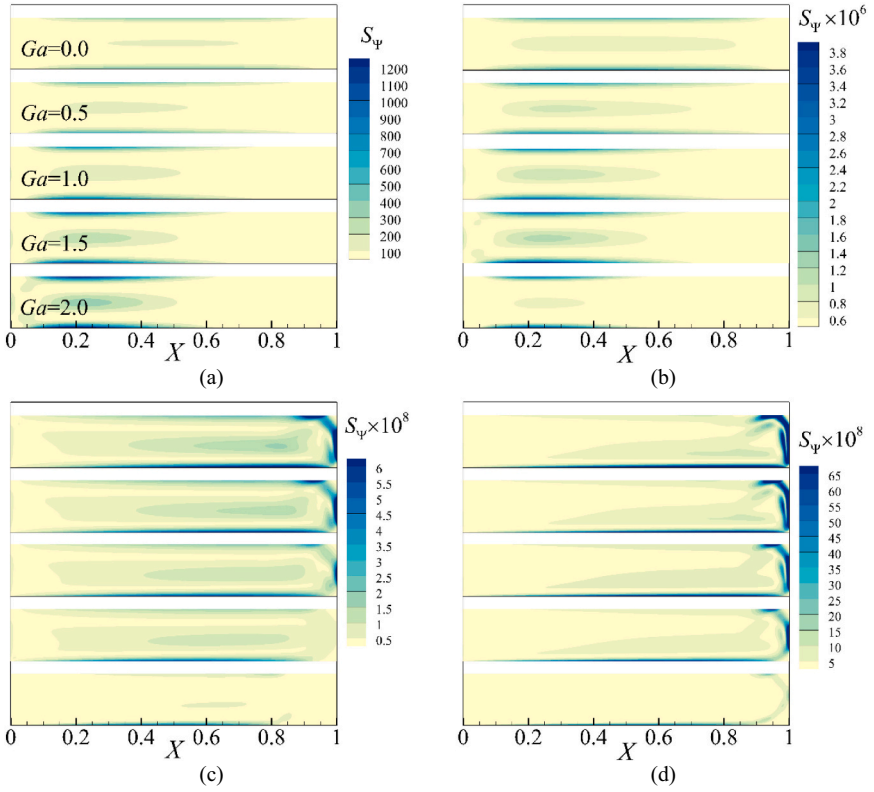

Fig. 3. Distribution of S_ψ over the physical domain with different *Ga* as stated at different Rayleigh numbers including (a) $Ra = 10^4$ (b) $Ra = 6 \times 10^5$ (c) $Ra = 4 \times 10^7$ and (d) $Ra = 4 \times 10^8$. Minimum and maximum of S_ψ are set equal in different frames of each figure.

weakening regions of most extreme vorticity in the flow, in turn weakening their contribution to S_ψ. Results at $Ra = 4 \times 10^8$ (Fig. 3d) further demonstrate the shift of S_ψ from the horizontal boundaries and interior to the plume region; here the low-*Ga* plume region dominates the distribution of S_ψ.

The influence of the end-wall plume region is further investigated by calculating the magnitude of the non-Boussinesq term, i.e. $|Ga\Theta((U \cdot \nabla)U)|$, over the physical domain in the convection-dominated regime at $Ra = 4 \times 10^7$ and 4×10^8 in Fig. 4. This term acts as a modifier through the advection part of momentum equation. As seen, stronger non-Boussinesq effects are visible across the plume region by increasing both *Ga* and *Ra*. The observed trend in the S_ψ irreversibilities at $Ra = 4 \times 10^7$ and 4×10^8 (Fig. 3c and d) by increasing *Ga* may be attributed to the presented non-Boussinesq effects in Fig. 4. For both cases, the non-Boussinesq effects are strongest at $Ga = 1$ and it progressively weakens by increasing *Ga*. Overlaid stream-lines of the $Ga\Theta((U \cdot \nabla)U)$ provide a topological perspective on the action of this term, which is apparently towards a focal point that migrates from near the upper right corner of the enclosure at $Ga = 0.5$ towards a more central position as *Ga* is increased; this correlates with the alleviation in S_ψ in the right side-wall plume as *Ga* is increased.

Local irreversibilities due to heat transfer (S_Θ) are portrayed in Fig. 5. Since three surfaces are thermally insulated, thermal conductive effects are important across the bottom boundary compared to the other boundaries. In the conduction-dominated regime (Fig. 5a), this effect is more tangible at the two bottom corners where the maximum

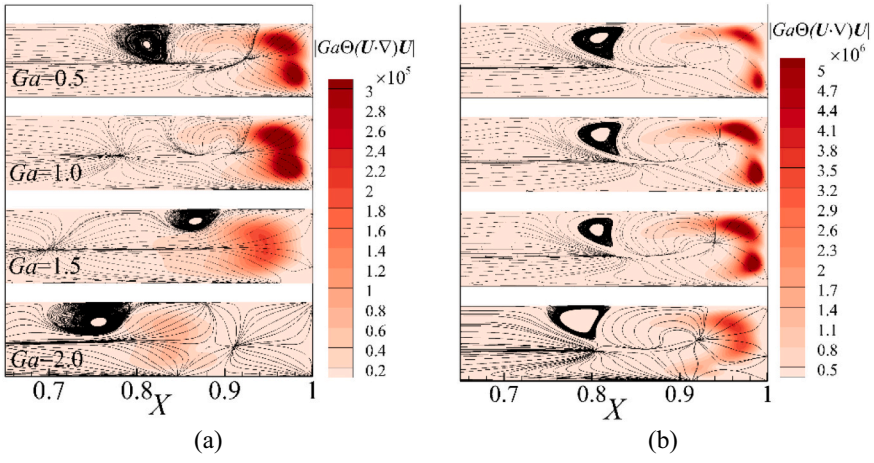

Fig. 4. Magnitude of the non-Boussinesq term ($|Ga\Theta((U \cdot \nabla)U)|$) over right-half of the physical domain at different *Ga* as stated in the convection-dominated regime (a) $Ra = 4 \times 10^7$ and (b) $Ra = 4 \times 10^8$.

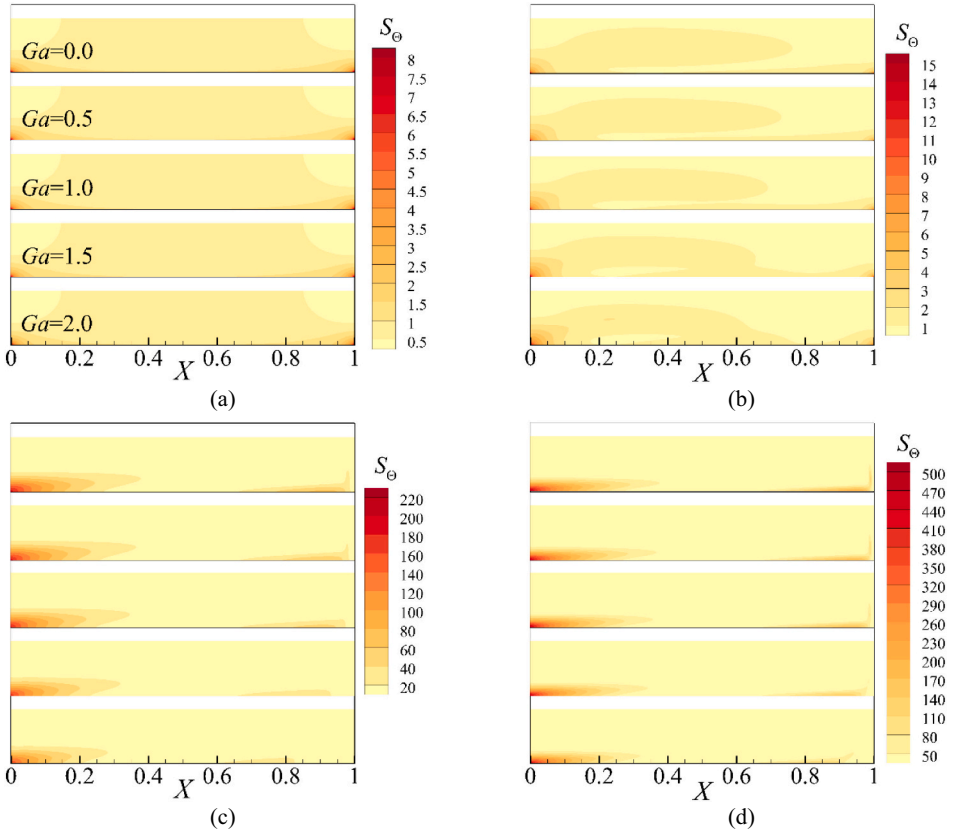

Fig. 5. Distribution of S_Θ over the physical domain with different Ga as stated at different Rayleigh numbers including (a) $Ra = 10^4$ (b) $Ra = 6 \times 10^5$ (c) $Ra = 4 \times 10^7$ and (d) $Ra = 4 \times 10^8$. Minimum and maximum of S_Θ are set equal in different frames of each figure.

temperature differences due to applied linear temperature distribution across the base. As can be seen, the Ga-dependence on the S_Θ distribution is visible in the conduction-dominated regime, and also at $Ra = 1.5 \times 10^5$ (Fig. 5b). By increasing the Rayleigh number (Fig. 5c and d), conduction effects become isolated to the cooling section of the boundary. This is consistent with Rayleigh—Bénard convection in which a cooling substrate located at the bottom side of the system de-energizes the fluid via conduction [35]. In the convection-dominated regime, this region extends further along the cooling section of the bottom boundary as thermal conduction is progressively superseded by convective heat transport at these higher Rayleigh number. A weak Ga-dependence can be seen in Fig. 5c and d, where the S_Θ strong zones shown by dark color, exhibit slightly different lengths as Ga is increased. In other words, different frames of Fig. 5c and d show negligible sensitivity to Ga alteration in this regime.

The local Bejan number distribution for different cases is presented in Fig. 6. As expected, in the conduction-dominated regime at $Ra = 10^4$ (Fig. 6a), computed Be_{loc} is almost uniformly distributed over the domain with a value close to unity, and variation in Ga has no effect. An interesting feature of the local Bejan number is noticed at $Ra = 6 \times 10^5$, where the average Bejan number is close to 0.5 for $Ga \gtrsim 0.5$ in Fig. 2c and the local Bejan number represents a general balance between S_ψ and S_Θ in Fig. 6b for mentioned values of Ga, with $Be_{loc} > 0.5$ indicating $S_\Theta > S_\psi$ and vice versa for $Be_{loc} < 0.5$. As mentioned before, S_Θ and S_ψ represent local irreversibilities due to heat conduction and viscous heat dissipation that correlates with velocity gradients. When the local Bejan number takes a value of 0.5, it means conduction and convection have the same power at that point. At this Rayleigh number the flow is convection-dominated at $Ga = 0$ but for $Ga \gtrsim 0.5$, conduction is dominant across the two bottom corners of the enclosure where the temperature difference is maximum and two parallel stretched cores close to the horizontal boundaries. As can be seen, the region under the influence of conduction expands over the heating section by increasing the Ga. On the other hand, the local Bejan number distribution shows a convection-dominated regime along the forcing boundary layer in the range of $0.15 \lesssim X \lesssim 0.65$ and a similar region along the top boundary that shrinks by increasing the Ga. These are the regions where the fluid is compelled to move due to buoyancy forces and to deflect vertically due to confining boundaries. A convection-dominated regime is also observed in the upper-half of the plume region at $Ga = 0.5$ that is annihilated by increasing Ga. A similar region exists at the top-left corner where the flow has to rotate, however part of the rotation is under the effect of cooling section that makes heat conduction as the dominant part of the heat transfer mechanism.

At $Ra = 4 \times 10^7$ and 4×10^8 (Fig. 6c and d), the whole flow is dominated by viscous entropy generation associated with convection except in the lower-left region where conductive cooling occurs. Comparing different frames of Fig. 6d indicates that by increasing Ga in the convection-dominated regime, the conduction effects become more important across the cooling section and stronger across the overturning plume region. The lowest local Bejan numbers are found adjacent to the right-hand side wall and along the top boundary. This reflects the fast convective flow upward in the buoyancy plume, which then progresses leftward along the top boundary; this is the return region of the overturning circulation. Ultimately, diffusive cooling at the left end takes over as described in [10].

5. Conclusion

An entropy generation analysis of horizontal convection under the centrifugal buoyancy approximation was conducted at unity Prandtl number for the first time to map different conduction and convection dominated regimes in terms of the irreversibilities due to heat transfer and fluid friction associated with the local and average Bejan number.

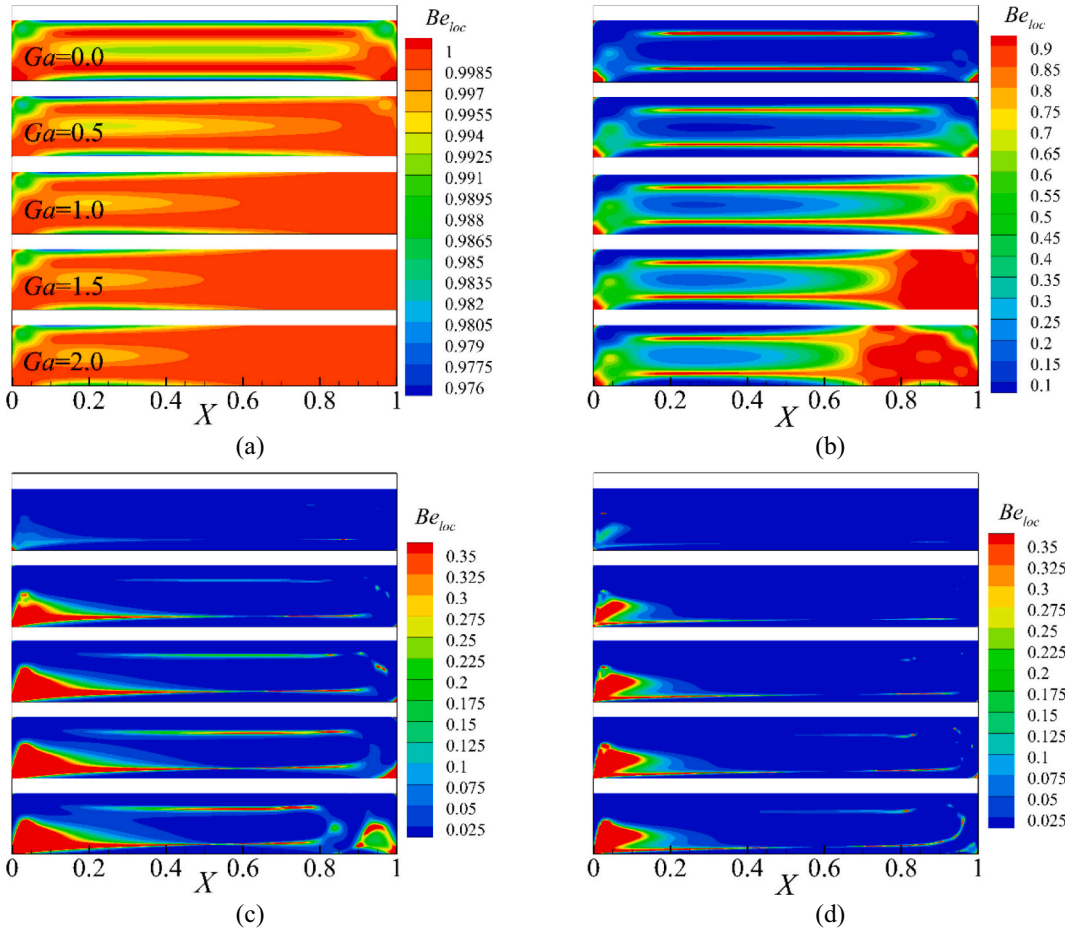

Fig. 6. Distribution of Be_{loc} over the physical domain with different Ga as stated at different Rayleigh numbers including (a) $Ra = 10^4$ (b) $Ra = 6 \times 10^5$ (c) $Ra = 4 \times 10^7$ and (d) $Ra = 4 \times 10^8$. Minimum and maximum of Be_{loc} are set equal in different frames of each figure.

The following items were the important findings/novelty of this study:

- The irreversibility distribution ratio is expressed using the Brinkman number and the Gay-Lussac parameter for the first time ($\chi = Br/Ga$).
- Entropy generation analysis was performed with a variable irreversibility distribution ratio at a fixed Brinkman number of $Br = 2 \times 10^{-5}$ and different Gay-Lussac parameters ranging $0 \leq Ga \leq 2$ up to $Ra = 5 \times 10^8$.
- At $Ra \approx 6 \times 10^5$ for $Ga \gtrsim 0.5$, the average Bejan number crosses with $Be_{ave} = 0.5$ where conduction and convection heat transfer mechanisms are in balance.
- The transition of the average Bejan number from conduction to convection-dominated regime follows closely to reciprocal ($Be_{ave} \sim Ra^{-1}$) for $Ga = 0$ but the same process occurs with $Be_{ave} \sim Ra^{-0.5}$ relation at $Ga = 2$.
- Ga has almost no role/effect on the buoyancy-driven flow field in the conduction-dominated regime ($Ra \lesssim 10^4$) but it expands regions under the influence of heat conduction in the convection-dominated regime.

Declaration of Competing Interest

No deceleration of interest.

Acknowledgements

This research was supported by the Australian Research Council through Discovery Project DP180102647. P. M. is supported by a Monash Graduate Scholarship and a Monash International Postgraduate Research Scholarship. The authors are also supported by time allocations on the National Computational Infrastructure (NCI) peak facility and the Pawsey Supercomputing Centre through NCMAS grants. NCI is supported by the Australian Government.

References

[1] T.K. Tsai, W.K. Hussam, M.P. King, G.J. Sheard, Transitions and scaling in horizontal convection driven by different temperature profiles, Int. J. Therm. Sci. 148 (2020), 106166.
[2] K. Brayn, M.D. Cox, A numerical investigation of the oceanic general circulation, Tellus 19 (1) (1967) 54–80.
[3] B.J. Foley, D. Bercovici, W. Landuyt, The conditions for plate tectonics on super-Earths: Inferences from convection models with damage, Earth Planet. Sci. Lett. 331-332 (2012) 281–290.
[4] H.J.J. Gramberg, P.D. Howell, J.R. Ockendon, Convection by a horizontal thermal gradient, J. Fluid Mech. 586 (2007) 41–57.
[5] H.T. Rossby, On thermal convection driven by non-uniform heating from below: an experimental study, Deep Sea Res. Oceanogr. Abstr. 12 (1965) 9–16.
[6] J.H. Siggers, R.R. Kerswell, N.J. Balmforth, Bounds on horizontal convection, J. Fluid Mech. 517 (2004) 55–70.
[7] G.J. Sheard, M.P. King, Horizontal convection: effect of aspect ratio on Rayleigh-number scaling and stability, Appl. Math. Model. 35 (4) (2011) 1647–1655.
[8] O. Shishkina, S. Grossmann, D. Lohse, Heat and momentum transport scalings in horizontal convection, Geophys. Res. Lett. 43 (2016) 1219–1225.
[9] S. Grossmann, D. Lohse, Scaling in thermal convection: a unifying theory, J. Fluid Mech. 407 (2000) 27–56.
[10] G.O. Hughes, R.W. Griffiths, Horizontal convection, Annu. Rev. Fluid Mech. 40 (2008) 185–208.
[11] J.M. Lopez, F. Marques, M. Avila, The Boussinesq approximation in rapidly rotating flows, J. Fluid Mech. 737 (2013) (2013) 56–77.
[12] T. Pesso, S. Piva, Laminar natural convection in a square cavity: low Prandtl numbers and large density differences, Int. J. Heat Mass Transf. 52 (3-4) (2009) 1036–1043.

[13] P. Mayeli, G. J. Sheard, An efficient and simplified Gay-Lussac approach in secondary variables form for the Non-Boussinesq simulation of free convection problems. Int. J. Numer. Methods Fluids 93 (11), 3264-3279.
[14] P. Mayeli, G. J. Sheard, A simplified and efficient Gay-Lussac approach for non-Boussinesq treatment of natural convection problems. Numer. Heat Transf. B 80 (5-6), 115-135.
[15] P. Mayeli, G.J. Sheard, A centrifugal buoyancy formulation for Boussinesq-type natural convection flows applied to the annulus cavity problem, Int. J. Numer. Methods Fluids 93 (3) (2021) 683–702.
[16] P. Mayeli, G.J. Sheard, Natural convection and entropy generation in square and skew cavities due to large temperature differences: a Gay-Lussac type vorticity stream-function approach, Int. J. Numer. Methods Fluids 93 (7) (2021) 2396–2420.
[17] P. Mayeli, G.J. Sheard, Buoyancy-driven flows beyond the Boussinesq approximation: a brief review, Int. Commun. Heat Mass Transf. 125 (2021), 105316.
[18] P. Mayeli, T.K. Tsai, G.J. Sheard, Linear stability analysis of horizontal convection under a Gay-Lussac type approximation, Int. J. Heat Mass Transf. 182 (2022), 121929.
[19] G. Huminic, A. Huminic, Entropy generation of nanofluid and hybrid nanofluid flow in thermal systems: a review, J. Mol. Liq. 302 (2020), 112533.
[20] T. Tayebi, A.J. Chamkha, Entropy generation analysis due to MHD natural convection flow in a cavity occupied with hybrid nanofluid and equipped with a conducting hollow cylinder, J. Therm. Anal. Calorim. 139 (2020) 2165–2179.
[21] T. Tayebi, A. Sattar Dogonchi, N. Karimi, H. Ge-JiLe, A.J. Chamkha, Y. Elmasry, Thermo-economic and entropy generation analyses of magnetic natural convective flow in a nanofluid-filled annular enclosure fitted with fins, Sustain. Energy Technol. Assess. 46 (2021), 101274.
[22] T. Tayebi, H.F. Öztop, Entropy production during natural convection of hybrid nanofluid in an annular passage between horizontal confocal elliptic cylinders, Int. J. Mech. Sci. 171 (2020) 105378.
[23] T. Tayebi, H.F. Öztop, A.J. Chamkha, Natural convection and entropy production in hybrid nanofluid filled-annular elliptical cavity with internal heat generation or absorption, Therm. Sci. Eng. Prog. 19 (2021), 100605.
[24] S. Dutta, N. Goswami, A.K. Biswas, S. Pati, Numerical investigation of magnetohydrodynamic natural convection heat transfer and entropy generation in a rhombic enclosure filled with Cu-water nanofluid, Int. J. Heat Mass Transf. 136 (2019) 777–798.
[25] A.I. Alsabery, T. Tayebi, R. Roslan, A.J. Chamkha, I. Hashim, Entropy generation and mixed convection flow inside a wavy-walled enclosure containing a rotating solid cylinder and a heat source, Entropy 22 (2020) 606.
[26] A.K. Hussein, Entropy generation due to the transient mixed convection in a three-dimensional right-angle triangular cavity, Int. J. Mech. Sci. 146-147 (2018) 141–151.
[27] A.A.A.A. Al-Rashed, K. Kalidasan, L. Kolsi, R. Velkennedy, A. Aydi, A.K. Hussein, E. H. Malekshah, Mixed convection and entropy generation in a nanofluid filled cubical open cavity with a central isothermal block, Int. J. Mech. Sci. 135 (2018) 362–375.
[28] K. Ghachem, L. Kolsi, C. Mâatki, A.K. Hussein, M.N. Borjini, Numerical simulation of three-dimensional double diffusive free convection flow and irreversibility studies in a solar distiller, Int. Commun. Heat Mass Transf. 39 (2012) 869–876.
[29] A.K. Hussein, K. Lioua, R. Chand, S. Sivasankaran, R. Nikbakhti, D. Li, B.M. Naceur, B.A. Habib, Three-dimensional unsteady natural convection and entropy generation in an inclined cubical trapezoidal cavity with an isothermal bottom wall, Alex. Eng. J. 55 (2016) 741–755.
[30] A. Al-Rashed, L. Kolsib, A.K. Hussein, W. Hassen, M. Aichouni, M.N. Borjini, Numerical study of three-dimensional natural convection and entropy generation in a cubical cavity with partially active vertical walls, Case Stud. Therm. Eng. 10 (2017) 100–110.
[31] S. Dutta, N. Goswami, A.K. Biswas, S. Pati, Natural convection heat transfer and entropy generation inside porous quadrantal enclosure with nonisothermal heating at the bottom wall, Numer. Heat Transf. A 73 (2018) 222–240.
[32] S. Dutta, N. Goswami, A.K. Biswas, S. Pati, Natural convection heat transfer and entropy generation in a porous rhombic enclosure: influence of non-uniform heating, J. Therm. Anal. Calorim. 144 (2021) 1493–1515.
[33] S. Bhardwaj, A. Dalal, S. Pati, Influence of wavy wall and non-uniform heating on natural convection heat transfer and entropy generation inside porous complex enclosure, Energy 79 (2015) 467–481.
[34] A. Bejan, A study of entropy generation in fundamental convective heat transfer, J. Heat Transf. 10 (1979) 718–725.
[35] P. Kaur, R. Ganesh, Negative entropy-production rate in Rayleigh-Bénard convection in two-dimensional yukawa liquids, Phys. Rev. 39 (2012) 869–876.